Band edge alignment of pseudomorphic GaAs$_{1-y}$Sb$_y$ on GaAs

J.-B. Wang,* S. R. Johnson, S. A. Chaparro,[†] D. Ding, Y. Cao, Yu. G. Sadofyev, and Y.-H. Zhang
Department of Electrical Engineering & Center for Solid State Electronics Research, Arizona State University,
Tempe, Arizona 85287, USA

J. A. Gupta
Institute for Microstructural Sciences, National Research Council Canada, Ottawa, K1A 0R6, Canada

C. Z. Guo
Department of Physics, Peking University, Beijing 100871, People's Republic of China
(Received 25 August 2004; published 24 November 2004)

Measurements of the transition energies of GaAsSb quantum well samples with different barrier configurations reveal that the conduction band offset of the coherently strained GaAs$_{1-y}$Sb$_y$/GaAs heterojunction grown on GaAs has a zero crossing at a Sb mole fraction of $y=0.43\pm0.07$. A type-I band alignment is formed for lower Sb mole fractions and a type-II band alignment is formed for higher Sb mole fractions. This occurs as a consequence of a considerable amount (58%) of the -1.58 eV bandgap bowing being distributed to the conduction band. As a suitable active material for 1.3 µm emission, pseudomorphic GaAs$_{0.643}$Sb$_{0.357}$ grown on GaAs is determined to have a weak, 23 ± 23 meV, type-I conduction band offset and a bandgap energy of 928 ± 4 meV.

I. INTRODUCTION

The determination of band offsets of the GaAsSb/GaAs heterojunction is critical for theoretical modeling and device design. For example, GaAsSb grown on GaAs is one of the more promising active materials for GaAs substrate based, 1.3 µm vertical-cavity surface-emitting lasers,[1,2] which are of great importance for optical communication applications involving data links and optical interconnects. Both a weak type-I and a weak type-II band alignment for the GaAsSb/GaAs heterojunction have been reported;[2–13] from these measurements it is clear that a majority of the band offset occurs in the valance band resulting in a weak or almost flat conduction band alignment. Furthermore, typical measurements of the GaAsSb/GaAs band offset[2–13] rely on the determination of the electron-hole transition energy that for the most part depends on the bandgap energy which is much larger than the conduction band offset. Therefore, precise quantitative measurements of both the conduction band offset and the bandgap energy must be carried out in order to accurately determine the band alignment of GaAsSb/GaAs.

In this paper, we measure two sets of carefully designed quantum well (QW) samples with different barrier configurations to precisely determine the conduction band alignment of GaAsSb/GaAs with Sb mole fractions suitable for 1.3 µm emission. In this approach the position and height of electron barriers placed next to a GaAsSb active layer produce varying quantum confinement energy shifts that are sensitive to the size and type of the GaAsSb/GaAs conduction band offset. The resulting transition energy spectrum is fit to calculated results using the bandgap and the size and type of the conduction band alignment as fitting parameters. The modeling calculations are done using arbitrary conduction band offsets and bandgap values and consequently do not rely on any previous experimental or theoretical bandgap values.

This combined with multiple variable-barrier samples is the key to our novel and robust approach which we call variable barrier spectroscopy.

II. EXPERIMENT

In sample set A, a 7 nm thick GaAsSb layer is placed between two fixed 75 nm thick Al$_{0.50}$Ga$_{0.50}$As barriers with 5 nm thick variable height Al$_x$Ga$_{1-x}$As barrier spacers between the GaAsSb layer and the fixed barriers. Five samples were grown with various aluminum mole fractions, $x=0.0$, 0.1, 0.2, 0.3, and 0.4, resulting in conduction band barrier heights of $E_x=E_c(\text{Al}_x\text{Ga}_{1-x}\text{As})-E_c(\text{GaAs})=0$, 81, 162, 243, and 324 meV, respectively.[14,15] In sample set B, a 7 nm thick GaAsSb layer is placed between a set of fixed 75 nm thick Al$_{0.25}$Ga$_{0.75}$As barriers with GaAs spacers of various thicknesses placed between the GaAsSb layer and the fixed barriers. Six samples were grown with GaAs spacer widths, $d=0.0$, 1.0, 2.0, 3.0, 6.0, and 9.0 nm.

The samples were grown by solid-source molecular beam epitaxy using a VG V80H system outfitted with As and Sb valved crackers to control the flux of the mixed group-V active layers. In both cases the 5-layer QW systems were grown on top of a 400 nm thick GaAs buffer on n^+ (100) GaAs substrates and were capped with a 30 nm thick GaAs layer. The GaAs buffer and cap were grown at 590 °C and the substrate temperature was ramped down (up) without growth interruption during the first (second) 75 nm thick AlGaAs barrier to facilitate the much lower 480 °C growth temperature of the GaAsSb active region. The substrate heater thermocouple was linearly ramped between two calibrated setpoints that had been determined before the growth using pyrometry measurements of the bare GaAs substrate. During the GaAsSb layer growth, the group-V fluxes were

TABLE I. Run to run Sb mole fraction variation given by XRD measurements.

Sample Number	Sample set A		Sample set B	
	Al mole fraction	Sb mole fraction	GaAs spacer (nm)	Sb mole fraction
1	0.10	0.351±0.003	6.0	0.361±0.003
2	0.40	0.361±0.003	1.0	0.356±0.002
3	0.00	0.363±0.004	3.0	0.358±0.001
4	0.30	0.355±0.003	0.0	0.360±0.001
5	0.20	0.353±0.002	9.0	0.352±0.001
6	-	-	2.0	0.355±0.003

Sb/Ga=0.45 and As/Ga=0.90, which for a growth temperature of 480 °C results in a Sb mole fraction around 0.35 and a GaAsSb/GaAs QW emission wavelength around 1.3 μm. To achieve sharp mixed group-V interfaces during the growth of the GaAsSb layer, the Sb valve was opened ∼10 s before the Sb shutter was opened, to allow the Sb flux to stabilize before the GaAsSb layer was grown.

Knowledge of the Sb mole fraction in the GaAsSb layer is critical in analyzing the transition energy spectrum; therefore x-ray diffraction (XRD) measurements and theoretical fitting were done for each sample. The high-resolution XRD measurements were performed with a Philips MRD system using an asymmetric double-crystal, channel-cut monochromator and the Cu Kα_1 line. The measurements were acquired in 13-hour scans, with 18-arcsec steps and an acquisition time of 60 s per point, scanning in a standard $\theta/2\theta$ geometry about the GaAs (004) symmetric substrate Bragg reflection. The XRD measurements were fit with a genetic algorithm which determines the global best fit to a model calculated using dynamical XRD theory. Vegard's law is assumed such that the lattice constant of unstrained GaAs$_{1-y}$Sb$_y$ is linear in the mole fraction.

The GaAsSb mole fraction, the GaAs cap thickness, and the mole fractions of the two fixed 75 nm thick AlGaAs barriers were fitting parameters in the XRD modeling; all of the other parameters of the 5-layer QW structure were fixed at the nominal grown values, which are expected to be accurate within ±3% based on previous calibrations of the MBE system. Minimizing the number of fitting parameters avoids overfitting the XRD data as well as spurious parameter values caused by correlated parameters. Furthermore, only the mole fraction (and not the thickness) of the GaAsSb layer is extracted from the XRD analysis because (1) sensitivity analysis of the XRD data indicates that the Sb mole fraction and GaAsSb layer thickness are strongly correlated; and (2) sensitivity analysis of the QW energy spectrum indicates that the transition energies are an order of magnitude more sensitive to variations in the Sb mole fraction than to those in the GaAsSb layer thickness.

The Sb mole fraction values obtained from the XRD analysis are summarized in Table I. The 5 samples of set A (variable barrier height) have an average value of 0.357 with a high of 0.363±0.004 and a low of 0.351±0.003. The 6 samples of set B (variable spacer width) have an average

value of 0.357 with a high of 0.361±0.003 and a low of 0.352±0.001. These results indicate that the mixed group-V composition was reliably controlled during the growth of these samples, which is remarkable when one considers the sources of instabilities in the growth of mixed group-V materials. The growth is done under an excess group-V flux where the relative incorporation of Sb and As is very temperature dependent, for example, a 1 °C increase (decrease) in substrate temperature during the growth of GaAsSb decreases (increases) the Sb mole fraction by 0.001. In addition to the requirement that the substrate temperature be reproduced within a few degrees the As and Sb flux levels must be reproduced to within 1% to achieve these results.

To determine the ground state energy transition of each sample, photoluminescence (PL) measurements were carried out at room temperature using an argon-ion laser emitting at 514 nm with an excitation power density of 35 W/cm². The luminescence was measured using a high-resolution spectrometer, liquid nitrogen cooled germanium detector, and a computer controlled lock-in amplifier. Since the PL experiments were carried out at room temperature, exciton effects are small and have been neglected. Furthermore, excitation dependent measurements from 1 to 35 W/cm² show that the PL peak blue shifts by less than 0.5 meV for all samples, demonstrating that any blue shift due to excitation density differences caused by sample geometry is small and can be neglected. The ground-state energy transition is therefore reasonably assumed to coincide with the peak position of the PL spectrum.

III. THEORETICAL MODELING

The measured transition energies for each sample set are compared to a family of calculated transition energy curves to determine the most likely pseudomorphic bandgap and band offset values for each sample set. The band offset and bandgap values used in the calculations are chosen (independent of previous bandgap or band offset measurements) over a reasonable range of values that justify the observed transition energies. The calculated set of curves are reliable because the calculations only depend on the electron and heavy-hole confinement energy shifts based on arbitrary band alignment configurations of the quantum well system and do not depend on less reliable calculations, such as bandgap and band offset values based on empirical expressions and material strain calculations. In detail, the ground state transition energies are calculated for the two sample sets (A and B) using arbitrary GaAsSb/GaAs conduction band offsets, ΔE_c^{qw}=60, 40, and 20 meV for a type-I alignment; 0 meV for flat bands; and −20,−40, and −60 meV for a type-II alignment. The calculations are done using the transfer matrix method to solve a system of Schrödinger equations.[15] Band mixing, intraband relaxation scattering, and band-gap shrinkage are neglected, which is a valid approximation for low injection PL measurements. The effective electron and heavy-hole masses used in the calculations are given in Table II.

The calculated results for sample set A are plotted as solid circles in Fig. 1 for the case where the arbitrary preset band-

TABLE II. Material parameters, calculations, and experimental results.

Parameter	Symbol	GaAs	GaSb	GaAs$_{0.643}$Sb$_{0.357}$
lattice constant	$a(\text{Å})$	5.65325[a]	6.09593[a]	5.81129[a]
elastic stiffness constant ratio	C_{12}/C_{11}	0.4526[a]	0.4553[a]	0.4534[a]
hydrostatic deformation potentials	$a_c(\text{eV})$	−7.17[a]	−6.85[a]	−7.06[a]
	$a_\nu(\text{eV})$	1.16[a]	0.79[a]	1.03[a]
shear deformation potential	$b(\text{eV})$	−1.7[a]	−2.0[a]	−1.8[a]
electron effective mass	m_e/m_0	0.067[a]	0.0393[a]	0.0486[a]
heavy-hole effective mass	m_{hh}/m_0	0.5[a]	0.4[a]	0.471[a]
light-hole effective mass	m_{lh}/m_0	0.087[a]	0.05[a]	0.0738[a]
bulk bandgap energy (300K)	$E_g^{\text{bulk}}(\text{eV})$	1.424[a]	0.726[a]	0.782[c]
bulk conduction band offset	$\Delta E_c^{\text{bulk}}(\text{eV})$	-	0.018[a]	0.232[c]
bulk valence band offset	$\Delta E_\nu^{\text{bulk}}(\text{eV})$	-	−0.680[a]	−0.410[c]
strained bandgap energy	$E_g^{qw}(\text{eV})$	-	1.053[a]	0.928±0.004[b]
strained electron band offset	$\Delta E_c^{qw}(\text{eV})$	-	−0.524[a]	0.023±0.023[b]
strained heavy-hole band offset	$\Delta E_{\nu hh}^{qw}(\text{eV})$	-	−0.895[a]	−0.473±0.023[b]
strained light-hole band offset	$\Delta E_{\nu lh}^{qw}(\text{eV})$	-	−0.340[a]	−0.287[c]

[a]Values (or calculated using values) from Refs. 15,17,18.
[b]Measurements from this work.
[c]Calculated using measurements from this work and the Bir-Pikus Hamiltonian (Ref. 17).

gap energy is 935 meV, which is selected as a reasonable starting point by examination of the experimental data and the calculations. It is important to note that any other reasonable choice for the preset bandgap value for calculation purposes, essentially shifts the curves up or down in energy from those shown in Fig. 1, and does not affect the final outcome of the analysis. A result of the fact that the deep heavy-hole energy level is comparatively insensitive to small changes in the hole barrier height when selecting a slightly different preset bandgap value.

The solid curves shown in Fig. 1 are fits of the following equation to the calculated results:

$$E_{PL} = E_g^{qw}(\text{GaAsSb}) + 2E_a\left(\exp\left(\frac{E_x - E_b}{E_x + E_b} - 0.94\right) - 1\right)$$
$$+ 92.3 \text{ meV}. \tag{1}$$

During the fit, E_a and E_b are fitting parameters, while E_x is
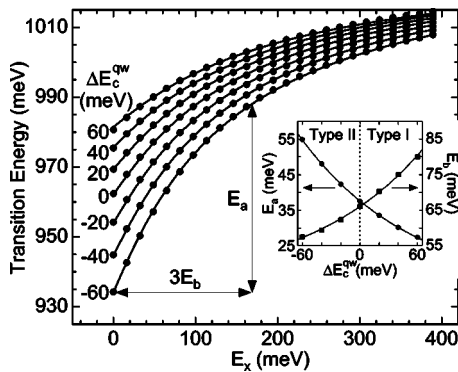
FIG. 1. Theoretical calculations and model of the transition energy versus the AlGaAs barrier height for various GaAsSb/GaAs conduction band offsets.

fixed at the experimental set of conduction band barrier heights discussed above and $E_g^{qw}(\text{GaAsSb})$ is fixed at the preset bandgap energy used in the calculations; note that $E_g^{qw}(\text{GaAsSb})$ is converted into a fitting parameter when the experimental data is analyzed. This procedure is used to parametrize the calculations in a functional form to facilitate the extraction of the bandgap and band offset from the experimental data. In this parametrization, each individual conduction band offset has a unique set of distinguishing energies E_a and E_b which only weakly depend ($<1/250$) on the present bandgap value when selected within the 900 to 970 meV range. Equation (1) is related to the band alignment by noting that E_a and E_b depend exponentially on the conduction band offset ΔE_c^{qw} with a characteristic energy, $E_0 = 118.6$ meV, as given in the following two equations and shown in the inset of Fig. 1:

$$E_a = 11.5 + 26.1 \cdot \exp\left(-\frac{\Delta E_c^{qw}}{E_0}\right) \text{ meV}, \tag{2}$$

$$E_b = 44.0 + 22.0 \cdot \exp\left(\frac{\Delta E_c^{qw}}{E_0}\right) \text{ meV}. \tag{3}$$

Physically, as illustrated in Fig. 1, the ground-state energy transition increases by E_a, when the conduction band barrier height, E_x, changes from 0 to $3E_b$. The size of this shift is strongly dependent on the band offset and is much larger when a type-II band alignment is present. The change in the transition-energy caused by the change in the barrier layer originates mainly (99.7%) from the conduction band, because the deep heavy-hole energy level is virtually unaffected by changes in the barrier layer. Therefore, from a practical point of view, the parameters depend on the quan-
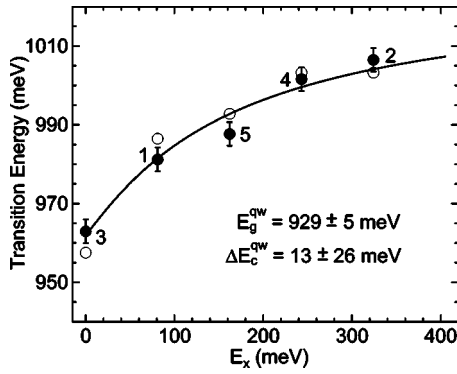
FIG. 2. Theoretical model fit to results for the variable AlGaAs barrier height experiment.

tum energy shifts in the conduction band, making this approach very sensitive to the size and the sign of the conduction band offset.

The experimental data for sample set A are plotted in Fig. 2 with the measured transition energies given by the open circles. Since the Sb mole fraction of the samples varies slightly (see Table I), the measured transition energies are adjusted for the run-to-run variations in the Sb mole fraction to improve the accuracy of the measurements. The solid circles in Fig. 2 give the transition energies shifted to those expected for a Sb mole fraction of exactly 0.357 (the average value for the sample set) using the following self-consistent fitting process. First, the bandgap and band offset is determined, assuming that the Sb mole fraction is the same average value for all samples. Using these values, the mole fraction dependence of the transition energy is determined, from which the transition energy for each sample is adjusted to the transition energy expected if a given sample had actually possessed the average Sb mole fraction value. Next, the bandgap and band offset are determined for the adjusted data set. This self-consistent process is repeated until the bandgap and band offset values converge. Since the Sb mole fraction variation was small, this process converged in the first iteration.

If we had not adjusted the experimental PL data for the sample to sample variation in the mole fraction, the inferred bandgap and band offset values would still be within the uncertainties reported. However, since the XRD measurements reveal a small variation in the sample to sample mole fraction, our best estimate of the bandgap and band offset must include this information. The error bars shown in Fig. 2 are determined from the uncertainty in the mole fraction given by the XRD measurements. Each data point is numbered in the order that the samples were grown; a random sequence was intentionally designed to minimize possible systematic errors. Equations (1) through (3) are fit to the adjusted experimental results with $E_g^{qw}(\text{GaAsSb})$ and ΔE_c^{qw} as fitting parameters. The best-fit parameters give the bandgap energy as $E_g^{qw}(\text{GaAsSb}) = 929 \pm 5$ meV and the conduction band offset as a weak type-I band alignment with $\Delta E_g^{qw} = 13 \pm 26$ meV for $\text{GaAs}_{0.643}\text{Sb}_{0.357}/\text{GaAs}$. The uncertainties reported here are 2 times the standard error ($\pm 2\sigma$) in the best-fit parameters given by the Levenberg-Marquart algorithm.[16]
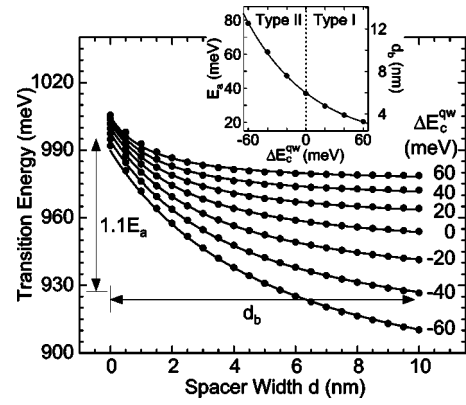
FIG. 3. Theoretical calculations and a model of the transition energy versus GaAs spacer width for various GaAsSb/GaAs conduction band offsets.

The calculations and investigation of sample set B follows the same procedures described above for sample set A, with the theoretical calculated results shown in Fig. 3 as the solid circles. The solid curves are parametrizations of the calculations using the following equation:

$$E_{PL} = E_g^{qw}(\text{GaAsSb}) + 2E_a\left(\exp\left(\frac{d_b - d}{d_b + d} - 1.14\right) - 1\right)$$
$$+ 74.9 \text{ meV}. \tag{4}$$

During the fit, E_a and d_b are fitting parameters, while d is fixed at the experimental set of GaAs spacer widths discussed above and $E_g^{qw}(\text{GaAsSb})$ is fixed at the preset bandgap energy. Analogous to sample set A, each individual conduction band offset has a unique set of distinguishing parameters E_a and d_b which only weakly depend ($<1/350$) on the present bandgap value when selected within the 900 to 970 meV range. E_a and d_b are related by the constant 6.24 meV/nm and increase exponentially, with characteristic energy $E_0 = 68.8$ meV, as the conduction band offset, ΔE_c^{qw}, goes from type I to type II (see the inset of Fig. 3 and the following equations):

$$E_a = 7.8 + 29.5 \cdot \exp\left(-\frac{\Delta E_c^{qw}}{E_0}\right) \text{ meV}, \tag{5}$$

$$d_b = \frac{E_a}{6.24 \text{ meV}} \text{ nm}. \tag{6}$$

Physically, as illustrated in Fig. 3, the ground-state electron energy level is shifted up by $1.1\, E_a$ when the GaAs spacer width d changes from d_b to 0. Again the magnitude of this shift is strongly dependent on the band offset and is much larger when a type-II band alignment is present.

The experimental data for sample set B (numbered in the order that the samples were grown) are plotted in Fig. 4 with the measured transition energies given by the open circles and the measured transition energies adjusted for the run-to-run variation in the Sb mole fraction given by the solid circles. As was done for sample set A, the best estimate of the bandgap and band offset includes adjustment of transition
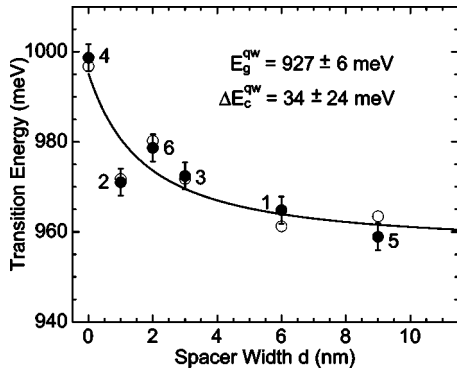
FIG. 4. Theoretical model fit to results for a variable GaAs spacer width experiment.

FIG. 5. Band-edge diagram of 5-layer quantum-well structures with variable AlGaAs barrier height shown in (a) and variable GaAs spacer width shown in (b).

energies to those expected for a Sb mole fraction of exactly 0.357, the average value for sample set B. Equations (4) through (6) are fit to the experimental data with E_g^{qw}(GaAsSb) and ΔE_c^{qw} as fitting parameters. The best-fit parameters give the bandgap as E_g^{qw}(GaAsSb)$=927\pm6$ meV and the conduction band offset as weak type I with $\Delta E_c^{qw}=34\pm24$ meV for GaAs$_{0.643}$Sb$_{0.357}$/GaAs.

To confirm that the choice of the preset bandgap value for the calculations does not affect the outcome of the fit, the same series of calculations and fits performed above are repeated using preset bandgap values (900 and 970 meV) that are substantially away from the best-fit value. These new fits are also shown in Figs. 2 and 4 and are indistinguishable from the original fit for a preset bandgap value of 935 meV. The results of this analysis are summarized in Table III with the determined bandgap and band offset reported to a precision of 0.1 meV to resolve the differences. The choice of the preset bandgap value at most changes the best-fit bandgap and band offset values by ±0.1 meV well within the uncertainties reported here; demonstrating the robustness of this approach.

The bandgap and conduction band offset values obtained from sample sets A and B agree to within uncertainties. As a best estimate, the average values from the two sample sets ($E_g^{qw}=928\pm4$ meV and $\Delta E_c^{qw}=23\pm23$ meV) are reported in Table II, where the uncertainty is given as 2 times the standard error. The resulting band edge diagrams for the 5-layer QW structures are shown in Fig. 5. Where Fig. 5(a) gives the variable barrier height structure showing the bandgap energy

TABLE III. Pseudomorphic bandgap and conduction band offset for different present GaAsSb bandgap values.

	Preset bandgap (meV)	Determined bandgap (meV)	Determined band offset (meV)
Sample set A	900	929.3±4.8	12.8±26.2
	935	929.3±4.8	12.8±26.2
	970	929.4±4.8	12.9±26.2
Sample set B	900	926.9±5.6	33.8±23.8
	935	927.0±5.6	33.8±23.8
	970	927.1±5.6	33.9±23.8
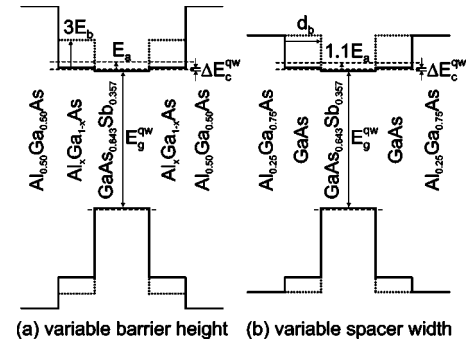
and the conduction band offset, an increase in the barrier height (dotted line) and the resulting confinement energy shift (dashed line), and the parameters E_a and E_b. Similarly, Fig. 5(b) gives the variable spacer width structure showing a decrease in the spacer width (dotted line) and the resulting confinement energy shift (dashed line) and the model parameters E_a and d_b. Note that in both structures the confinement energy shift essentially occurs in the conduction band because the deep heavy-hole level is insensitive to the variations in the band edge configuration.

Sensitivity analysis was performed to estimate the impact that the uncertainty in the MBE system calibration may have on the above measurements. In the worst case, the uncertainty in the transition energy is ±0.4 meV for a $\pm3\%$ uncertainty in the barrier layer Al composition (sample set A) and ±0.2 meV for a $\pm2\%$ uncertainty in spacer layer thickness (sample set B). The uncertainties given are based on GaAs and AlAs growth rate calibrations. Even if the growth rate uncertainty is doubled, the uncertainty in the transition energy is still less than 1 meV and hence well within the uncertainties reported in this work. Furthermore, if these errors are randomly applied (the worst case for the band offset measurement) the uncertainty in the measurement of the band offset is at most ±0.5 meV; again well within the uncertainties reported here. The uncertainties in the x direction (due to the growth calibration) are smaller than the size of the data points and are not shown in Figs. 2 and 4.

The bulk bandgap and band offsets are estimated from the pseudomorphic GaAs$_{0.643}$Sb$_{0.357}$ on GaAs measurements using the widely accepted Bir-Pikus Hamiltonian.[17] The bulk material values and the deformation potentials used in the calculation are listed in Table II. The uncertainty in the calculated bulk material values is relatively large (approximately $\pm10\%$) because the deformation potentials are not accurately known.[9,14] The calculated strained light-hole band offset is included in Table II for completeness.

IV. EMPIRICAL BAND EDGE MODEL

Assuming a simple parabolic bowing relation for the GaAsSb band edges, the bandgap, conduction band edge, and valence band edge for bulk and strained GaAs$_{1-y}$Sb$_y$ as a function of the Sb mole fraction are given in Eq. (7):

TABLE IV. Calculated and experimentally determined parameters.

Parameter	Symbol	strained, *qw*	*bulk*	Bir-Pikus, *ε*
Bandgap bowing	b_g^j(eV)	−1.58[c]	−1.71[c]	0.13[b]
Conduction band bowing	b_c^j(eV)	−0.91[c]	−0.98[c]	0.07[b]
Valence band bowing, heavy hole	b_{vhh}^j(eV)	0.67[c]	0.73[c]	−0.06[b]
Valence band bowing, light hole	b_{vlh}^j(eV)	0.72[c]	0.73[c]	−0.01[b]
Binary bandgap offset	Δ_g^j(eV)	0.371[b]	0.698[a]	−0.327[b]
Binary conduction band offset	Δ_c^j(eV)	−0.524[b]	0.018[a]	−0.542[b]
Binary heavy-hole band offset	Δ_{vhh}^j(eV)	−0.895[b]	−0.680[a]	−0.215[b]
Binary light-hole band offset	Δ_{vlh}^j(eV)	−0.340[b]	−0.680[a]	0.340[b]

[a]From Refs. 15,17,18.
[b]Calculated using the Bir-Pikus Hamiltonian (Ref. 17).
[c]Calculated using the measurements from this work.

$$E_i^j(\mathrm{GaAs}_{1-y}\mathrm{Sb}_y) = E_i^j(\mathrm{GaAs}) - \Delta E_i^j,$$

$$\text{with } i = g,c,v_{hh,lh} \text{ and } j = \text{bulk},qw,\varepsilon,$$

$$\text{where } \Delta E_i^j = \Delta_i^j \cdot y - b_i^j \cdot y \cdot (1-y),$$

$$\text{with } \Delta_i^j \equiv E_i^j(\mathrm{GaAs}) - E_i^j(\mathrm{GaSb}). \quad (7)$$

The relations between the bandgap and the conduction and valence band edges are

$$E_g^j = E_c^j - E_\nu^j, \quad \text{with } \Delta_g^j = \Delta_c^j - \Delta_\nu^j \text{ and } b_g^j = b_c^j - b_\nu^j. \quad (8)$$

And the relations between the parameters of the strained QW layer and bulk material are

$$E_i^{qw} = E_i^{\text{bulk}} + E_i^\varepsilon, \ \Delta_i^{qw} = \Delta_i^{\text{bulk}} + \Delta_i^\varepsilon \text{ and } b_i^{qw} = b_i^{\text{bulk}} + b_i^\varepsilon. \quad (9)$$

The constants b_i^j and Δ_i^j are the bowing parameters and the end point offset of the curves, respectively. The subscript *i* denotes the bandgap (*g*), the conduction band (*c*), or the valence band (*ν*) and the superscript *j* denotes bulk material (*bulk*), a strained QW layer (*qw*), or the energy shift due to strain (*ε*). The additional valence band subscripts refer to the splitting of the heavy-hole (*hh*) and the light-hole (*lh*) bands when strain is present. When used alone, *ν* refers to the lowest energy state for the holes, which is the heavy-hole band in the present compressively strained material system.

The simple relation in Eq. (7) between strained and bulk material arises because in addition to the strong bowing parameter in bulk GaAsSb the effects of strain through the Bir-Pikus Hamiltonian can be accurately described to second order in the Sb mole fraction. The values for the parameters in Eq. (7) are listed in Tables II and IV. The values obtained from, or calculated from values in the literature[15,17,18] are denoted [a] in Tables II and IV, the values measured in this work are denoted [b] in Table II, the values calculated from the literature using the Bir-Pikus Hamiltonian are denoted [b] in Table IV, and the values calculated using the results from this work are denoted [c] in Tables II and IV. Note that the measured values report are an average of the values obtained from the two sample sets.

The conduction and valence band (heavy-hole) edges for strained GaAs$_{1-y}$Sb$_y$ on GaAs are shown in Fig. 6. An examination of Fig. 6 and Eq. (7) shows that the band alignment of the GaAs$_{1-y}$Sb$_y$/GaAs heterojunction has a type-I to type-II crossover at a Sb mole fraction $y = (1 - \Delta_c^{qw}/b_c^{qw}) = 0.43 \pm 0.07$. The maximum in the conduction offset, $\Delta E_c^{qw} = (\Delta_c^{qw} - b_c^{qw}) \cdot (1 - \Delta_c^{qw}/b_c^{qw})/4 = 41 \pm 18$ meV, occurs at $y = (1 - \Delta_c^{qw}/b_c^{qw})/2 = 0.21 \pm 0.03$. The uncertainties reported here are determined from the uncertainty in the band offset measurement, assuming a simple bowing model with fixed binary endpoints. It is important to note that the calculated band offset at the GaSb endpoint has some uncertainty associated with it as well, coming mainly from the uncertainty in the value of GaSb deformation potential. Using the scatter of the deformation potential values in the literature, the uncertainty in the calculated GaSb endpoint is estimated to be about ±40 meV, which if included would increase the uncertainties in the critical points of the conduction band by about 10%.

V. DISCUSSION

One of the important contributions of this work is the quantification of the band bowing distribution which eliminates the need for an arbitrary assignment of the bandgap bowing to the valence band[7] or to the conduction band.[19] The
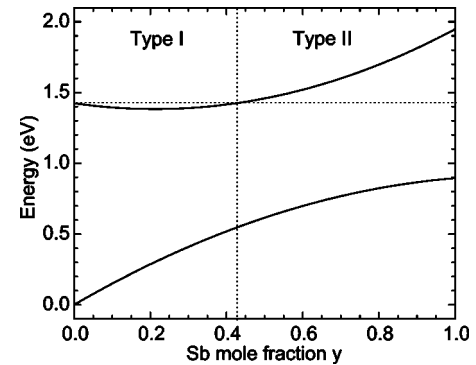
FIG. 6. Composition dependence of the conduction and heavy-hole band edges for pseudomorphic GaAs$_{1-y}$Sb$_y$ on GaAs.

present study indicates that the bandgap bowing of strained GaAsSb on GaAs is fairly evenly distributed between the conduction band (58%) and valence band (42%). Furthermore, the band bowing parameters of the strained QW material are related to the bulk material band bowing and the bowing introduced by the Bir-Pikus Hamiltonian [see Eq. (9) and Table II] which also demonstrates a similar bowing distribution. The second order dependence of the Bir-Pikus Hamiltonian on the mole fraction originates from the product of parameters which are linearly interpolated in the mole fraction and from the second order dependence of strain on the mole fraction, using the conventional definition of strain.[15] For this material system, the band bowing of strained GaAsSb on GaAs is reduced because the bowing introduced by the strain opposes that of the bulk material. It is interesting to note that these competing effects are also observed in the bond lengths of strained alloy materials.[20]

The valence band offset ratio, Q_ν, has been introduced in the literature[21] as a constant to describe the band alignments of heterostructures, such as AlGaAs/GaAs, where the band edge energies vary linearly with composition. However, for materials that exhibit band bowing, Q_ν is a function of composition, as shown in the equation following, where Q_ν is given for a ternary material embedded in one of its constitute binaries, such as $In_yGa_{1-y}As$ in GaAs or $GaAs_{1-y}Sb_y$ in GaAs:

$$Q_\nu^{qw} \equiv \frac{\Delta E_\nu^{qw}}{\Delta E_g^{qw}} = \frac{\Delta_\nu^{qw} - b_\nu^{qw} \cdot (1-y)}{\Delta_g^{qw} - b_g^{qw} \cdot (1-y)}. \tag{10}$$

Here Q_ν is only constant when little or no bulk band bowing or strain is present, namely b_ν^{qw} and b_g^{qw} are very small, or when the bowing distribution is by chance identical to the band offset distribution of the binary constitutes ($b_\nu^{qw}/b_g^{qw} = \Delta_\nu^{qw}/\Delta_g^{qw}$). In either case $Q_\nu^{qw} = \Delta_\nu^{qw}/\Delta_g^{qw}$. Clearly for materials that exhibit substantial bowing, such as GaAsSb, it is desirable to parametrize the conduction and valance band edges in terms of constants rather than variable band offset ratios.

In the previous studies, the strained bandgap energy of $GaAs_{1-y}Sb_y$ is often obtained from the bulk bandgap using various bowing parameters and energy shifts due to strain using various deformation potentials in the Bir-Pikus Hamiltonian. The published bulk bandgap bowing parameters[14,22–27] of $GaAs_{1-y}Sb_y$ are quite scattered; where in early work[22–24] the reported bulk bowing parameters range from -1.0 eV to -1.2 eV for Sb mole fractions below 0.25, more recently,[25] -1.87 eV is given for mole fractions below 0.1, and very recently,[14,27] bowing parameters around -1.4 eV are given for a mole fraction around 0.5. The published deformation potentials for GaAs are quite scattered,[9,14] which results in substantial variations in the calculated band edge energy shifts. Therefore, the simultaneous determination of the strained bandgap with strained band offset is critical for an accurate determination of the band alignment of GaAsSb/GaAs. This is undoubtedly difficult to achieve from measurements of a single sample, however, is straight forward using the suitably designed sample sets presented here.

The accuracy of the conduction band edge shown in Fig. 6 is of paramount importance in determining the GaAsSb/GaAs band alignment. The accuracy of this curve away from the measured value (around 36% Sb) depends on the appropriateness of the simple bowing model and the accuracy of the bowing parameters which are subject to uncertainty introduced in calculating the band edges of coherently strained GaSb. Nevertheless, the bowing parameters presented in Table IV are in reasonable agreement with those reported in the literature. This work asserts both band alignment types for GaAsSb/GaAs, depending on the Sb mole fraction present. It is important to note that this is typical when the constituent binaries form a negative offset in the conduction band, $\Delta_c^{qw} < 0$, and a significant amount of negative bowing is present, $b_c^{qw} < \Delta_c^{qw}$, in which case the conduction band edge will exhibit the observed positive-curvature zero-crossing. On the other hand, for a material system where the constituent binaries form a positive offset, $\Delta_c^{qw} > 0$, and where a significant amount of positive bowing is present in the conduction band, $b_c^{qw} > \Delta_c^{qw}$, the conduction band edge will again form a zero crossing, but with the opposite curvature. A similar type of behavior could occur in the valence band of some material systems.

Various band alignments for the GaAsSb/GaAs material system have been presented in the literature. A weak type-I band alignment with the conduction band offset $\Delta E_c^{qw} \sim 35$ meV is reported[2,3] for Sb mole fractions of 0.12 and 0.30, respectively. A magneto-optical study[4] of GaAsSb/GaAs QWs concludes a weak type-I band alignment as well. On the other hand, there are several reports[5–11] of a type-II band alignment with Q_ν ranging from 1.05 to 2.1. Large excitation-dependent blue shifts in PL measurements from GaAsSb/GaAs[12] and GaAsSb/InGaAs[13] QWs have also been attributed to a type-II band alignment. In our experience, the PL blue shifts observed in highly strained QW materials are predominantly a result of spatial band filling caused by inhomogeneous composition, and are consequently inconclusive as regards the band alignment present. In the samples presented here, the GaAsSb QWs were intentionally grown 20 °C below the optimal growth temperature for device applications, in order to reduce strain driven Sb segregation and hence minimize the impact of inhomogeneous composition on the measurements. The samples presented here exhibit very small excitation-dependent blue shifts (<0.5 meV) for excitation densities from 1 to 35 W/cm^2.

Much of the previous work revolves around fitting Q_ν (or $Q_c = 1 - Q_\nu$) as a constant or in some cases as a composition-dependent function, where the strained bandgap of GaAsSb is deduced from an empirical expression for bulk bandgap and subsequently corrected for the strain induced energy shift using the Bir-Pikus Hamiltonian, while in many cases neglecting the significant uncertainty introduced by the uncertainty in the deformation potentials. In the present study we improve on previous work by using variable barrier spectroscopy measurements of multiple samples to simultaneously measure both the pseudomorphic bandgap of GaAsSb and the pseudomorphic conduction band offset of GaAsSb/GaAs. Notwithstanding the reliability of the binary band offsets, $\Delta_i^{qw} = \Delta_i^{bulk} + \Delta_i^\varepsilon$, obtained from the literature and

the Bir-Pikus Hamiltonian, our results give a thorough and accurate description of the $GaAs_{1-y}Sb_y/GaAs$ band alignments and bowing parameters of GaAsSb. Furthermore, the second-order empirical band-edge model given in Eqs. (7) through (9) is a consistent and thorough model developed to offer a simple and clear description of the compositional dependence of band edges.

The $GaAs_{0.643}Sb_{0.357}/GaAs$ bandgap and band offset results presented here agree with our previous work,[28] of 933 ± 6 meV and 19 ± 19 meV, respectively. In our previous work, the Sb mole fraction was not measured independently for each sample and therefore corrections for the run-to-run variations in the mole fraction were not included. Furthermore, in our previous work we underestimated the Sb mole fraction at about 30% for 1.3 μm emission using electron diffraction measurements, which resulted in an overestimation of the bowing parameters. Therefore the very accurate mole fraction measurements in this work provides a more accurate and reliable measurement of the GaAsSb bowing parameters.

In conclusion, experimental data fitting and theoretical modeling confirm that the conduction-band offset of the $GaAs_{1-y}Sb_y/GaAs$ heterojunction forms a relatively weak, 23 ± 23 meV, type-I alignment, for a Sb composition in the neighborhood of 36% where 1.3 μm emission is observed. Using a simple bowing model, the $GaAs_{1-y}Sb_y/GaAs$ conduction band offset is found to exhibit a zero crossing at the Sb mole fraction $y = 0.43 \pm 0.07$, forming a type-I band alignment at the lower Sb mole fractions and a type-II band alignment at the higher Sb mole fractions, which is a result of a substantial amount of negative band bowing (−0.91 eV) in the conduction band.

*Corresponding author. Electronic address: jbwang@asu.edu

†Presently at Lytek Corporation, 4717 East Hilton Avenue, Phoenix, Arizona 85034, USA.

[1] P. Dowd, S. R. Johnson, S. A. Feld, M. Adamcyk, S. A. Chaparro, J. Joseph, K. Hilgers, M. P. Horning, K. Shiralagi, and Y.-H. Zhang, Electron. Lett. **39**, 987 (2003).

[2] T. Anan, M. Yamada, K. Tokutome, S. Sugou, K. Nishi, and A. Kamei, Electron. Lett. **35**, 903 (1999).

[3] A. D. Prins, D. J. Dunstan, J. D. Lambkin, E. P. O'Reilly, A. R. Adams, R. Pritchard, W. S. Truscott, and K. E. Singer, Phys. Rev. B **47**, 2191 (1993).

[4] R. T. Senger, K. K. Bajaj, E. D. Jones, N. A. Modine, K. E. Waldrip, F. Jalali, J. F. Klem, G. M. Peake, X. Wei, and S. W. Tozer, Appl. Phys. Lett. **83**, 2614 (2003).

[5] G. Ji, S. Agarwala, D. Huang, J. Chyi, and H. Morkoc, Phys. Rev. B **38**, 10571 (1988).

[6] M. Peter, K. Winkler, M. Maier, N. Herres, J. Wagner, and K. H. Bachem, Appl. Phys. Lett. **67**, 2639 (1995).

[7] G. Liu, S.-L. Chuang, and S.-H. Park, J. Appl. Phys. **88**, 5554 (2000).

[8] M. Dinu, J. E. Cunningham, F. Quochi, and J. Shah, J. Appl. Phys. **94**, 1506 (2003).

[9] R. Teissier, D. Sicault, J. C. Harmand, G. Ungaro, G. Le Roux, and L. Largeau, J. Appl. Phys. **89**, 5473 (2001).

[10] Gh. Dumitras and H. Riechert, J. Appl. Phys. **94**, 3955 (2003).

[11] X. D. Luo, C. Y. Hu, Z. Y. Xu, H. L. Luo, Y. Q. Wang, J. N. Wang, and W. K. Ge, Appl. Phys. Lett. **81**, 3795 (2002).

[12] Y. S. Chiu, M. H. Ya, W. S. Su, and Y. F. Chen, J. Appl. Phys. **92**, 5810 (2002).

[13] W. W. Chow, O. B Spahn, H. C. Schneider, and J. E. Klem, IEEE J. Quantum Electron. **37**, 1178 (2001).

[14] I. Vurgaftman, J. R. Meyer, and L. R. Ram-Mohan, J. Appl. Phys. **89**, 5815 (2001).

[15] S.-L. Chuang, *Physics of Optoelectronic Devices* (Wiley, New York, 1995).

[16] W. H. Press, S. A. Teukolsky, W. T. Vetterling, and B. P. Flannery, *Numerical Recipes in FORTRAN, the Art of Scientific Computing* (Cambridge University Press, New York, 1992).

[17] G. E. Pikus and G. L. Bir, Sov. Phys. Solid State **1**, 1502 (1960).

[18] Y. Tsou, A. Ichii, and E. M. Garmire, IEEE J. Quantum Electron. **28**, 1261 (1992).

[19] C. G. Van de Walle, Phys. Rev. B **39**, 1871 (1989).

[20] J. C. Woicik, J. A. Gupta, S. P. Watkins, and E. D. Crozier, Appl. Phys. Lett. **73**, 1269 (1998).

[21] J. Menéndez, A. Pinczuk, D. J. Werder, A. C. Gossard, and J. H. English, Phys. Rev. B **33**, 8863 (1986).

[22] G. A. Antypas and L. W. James, J. Appl. Phys. **41**, 2165 (1970).

[23] M. B. Thomas, W. M. Coderre, and J. C. Woolley, Phys. Status Solidi A **2**, K141 (1970).

[24] R. E. Nahory, M. A. Pollack, J. C. DeWinter, and K. M. Williams, J. Appl. Phys. **48**, 1607 (1977).

[25] J. L. Castaño and J. Piqueras, J. Appl. Phys. **54**, 3433 (1983).

[26] J. F. Klem, D. Huang, H. Morkoc, Y. E. Ihm, and N. Otsuka, Proc. SPIE **877**, 28 (1988).

[27] R. Ferrini, M. Geddo, G. Guizzetti, M. Patrini, S. Franchi, C. Bocchi, F. Germini, A. Baraldi, and R. Magnanini, J. Appl. Phys. **86**, 4706 (1999).

[28] S. R. Johnson, C. Z. Guo, S. Chaparro, Yu. G. Sadofyev, J. Wang, Y. Cao, N. Samal, J. Xu, S. Q. Yu, D. Ding, and Y.-H. Zhang, J. Cryst. Growth **251**, 521 (2003).